On the use of electrochemical techniques to monitor free oxide content in molten fluoride media

Laurent Massot, Laurent Cassayre, Pierre Chamelot, Pierre Taxil

On the use of electrochemical techniques to monitor free oxide content in molten fluoride media

L. Massot*, L. Cassayre, P. Chamelot and P. Taxil

Université Paul Sabatier, Laboratoire de Génie Chimique UMR 5503,

Département Procédés Electrochimiques, 31062 Toulouse Cedex 9, France

(*) corresponding author:
Massot Laurent
Tel: +33 5 61 55 81 94
Fax: +33 5 61 55 61 39
e-mail: massot@chimie.ups-tlse.fr

Abstract

The electrochemical behaviour of oxide ions has been studied in fluoride melts (LiF/NaF eutectic) by cyclic voltammetry, square wave voltammetry and chronopotentiometry. The purpose is to determine whether these techniques can be used for titration of free oxide ions (O^{2-}) in molten fluorides released by lithium oxide additions. Cyclic voltammetry is shown to be unsuitable for this purpose due to oxygen bubbling disturbing the oxidation peak, while square wave voltammetry is far more appropriate because the observed signal is a well defined oxidation peak with a height proportional to the oxide content. Thus, the present work is focused on a strategy of oxide ions titration by square wave voltammetry. In addition, this work allows assessing that the electrochemical reduction of oxide ions proceeds by diffusion of these species, and the O^{2-} diffusion coefficient is estimated by chronopotentiometry.

Key words

Molten fluorides, gold electrode, oxide, square wave voltammetry, oxygen

Introduction

Numerous processes using molten salts media are influenced by the oxide ions content in the melt. Consequently, the management of the free oxide content of the melts during the process, preferably using a methodology adapted to an on-line implementation, is of great importance.

In molten chlorides media, potentiometric titration of oxide ions using the well-known Yttria Stabilised Zirconia Electrode (YSZE) was proposed by several authors [1-5]. This method is not valid in molten fluorides because of the instability of ZrO_2 and Y_2O_3 in these media.

In earlier works, our Laboratory implemented successfully a probe for titrating trivalent and divalent iron, chromium and sulphur in molten silicates at 1100°C based on square wave voltammetry (SWV) [6].

The method consists in measuring the reduction peak intensity obtained on the SWV voltammograms which was proved to be linear with the content of each species. Then, the content of these species in a given glass solution was determined using a calibration method. The accuracy of the results obtained by this methodology leaded us to build a probe allowing an on-line titration of the $Fe^{(III)}/Fe^{(II)}$ ratio in industrial glasses by measuring the ratio of SWV peaks of these species [7]. Similar results were obtained by our Laboratory for the titration of Niobium species in molten fluoride (Nb^{V} and Nb^{IV}) during the electrodeposition process of Nb metal [8]. In addition, the method was shown to be sensitive to determine the oxide ions content in the molten salts media [9].

Here, the SWV methodology is implemented for titrating O^{2-} ions using the electrochemical oxidation peak of oxide ions into gaseous oxygen on a gold electrode. Gold was selected as working electrode due to its high stability under oxygen evolution in molten media such as carbonates or cryolithe [10-12].

A preliminary investigation of the electrochemical behaviour of the gold electrode by several electrochemical techniques was realized in order to characterise the oxidation wave of O^{2-} ions.

2. Experimental

- The cell consisted in a vitreous carbon crucible placed in a cylindrical vessel made of refractory steel and closed by a stainless steel lid equipped with a jacket of circulating water for cooling. The inner part of the walls was protected against fluoride vapours by a graphite liner. The experiments were performed under an inert argon U atmosphere, previously dehydrated and deoxygenated using a purification cartridge (Air Liquide). The cell was heated using a programmable furnace and the temperatures were measured using a chromel-alumel thermocouple.

- The electrolytic bath used was the eutectic LiF/NaF (Merck 99.99%) mixture (60/40 mol%). It was initially dehydrated by heating under vacuum (10^{-2} mmHg) from ambient temperature up to its melting point (650°C) for 72 h.

- Electrodes: gold wire (0.5 mm diameter) was used as working electrode. The area of the working electrode was determined after each experiment by measuring the immersion depth in the bath. The auxiliary electrode was a vitreous carbon (V25) rod (3 mm diameter) with a large surface area (2.5 cm^2). The potentials were referred to a platinum wire (0.5 mm diameter) immersed in the molten electrolyte, which was proved to act as a quasi-reference electrode $Pt/PtO_x/O^{2-}$ [13], with a stable potential when the O^{2-} content is constant.

- Electrochemical equipment: all the electrochemical studies and electrolysis were performed with an Autolab PGSTAT30 potentiostat / galvanostat controlled by a computer using the research software GPES 4.9.

3. Results and discussion

3.1. Potential – oxoacidity diagram of oxide ions and gold compounds

Figure 1 exhibits, on a potential – oxoacidity diagram, the respective stability of oxygen and gold species as function of the potential and the oxide content in fluoride melts. This diagram was calculated at T = 827 °C and with soluble species activity of 0.1 $mol.kg^{-1}$, according to thermochemical data from Barin [14], and considering the following compounds: Li_2O, $O_{2\,(g)}$, Au, AuF_2, AuF_3 and Au_2O_3. The diagram shows that, whatever the concentration of O^{2-} in the melt, oxygen formation occurs at a lower potential than gold oxidation into AuF_2.

It can be concluded that, according to thermochemical calculations, the oxygen processing in fluoride melts can be performed on a gold electrode without any oxidation of the metal, as previously stated by Cassayre in cryolithe media [12].

3.2. Characterisation of the oxide ion oxidation mechanism in fluoride melts

3.2.1. Cyclic voltammetry

Cyclic voltammetry was used to identify the oxidation process of O^{2-} ions into oxygen in the LiF-NaF mixture. Before the addition of oxide ions in the melt, cyclic voltammetry was performed on a gold electrode at 800°C.

On Figure 2, the anodic part of a cyclic voltammogram obtained with a scan rate of 100 mV/s shows that the oxidation of gold electrode occurs at about 2.1 V/Pt. The reverse scan exhibits a cathodic peak obviously associated to the reduction of gold ions generated during the direct scan.

Small amounts of lithium oxide were then added in the bath, up to a content of 0.2 mol/kg. Figure 3 compares the cyclic voltammograms observed after each addition. It can be

noted on these voltammograms that the waves associated to the oxide ions are observed at a lower potential (1.1 V/Pt) than gold oxidation which was pointed out at 2.1 V/Pt. The current increase with the oxide content increase confirms that these waves can be attributed to the oxidation of O^{2-} ions; one can observe two parts on the voltammograms: (i) the beginning part of the wave (from 1.0 to 1.3 V/Pt) has a regular shape, (ii) from 1.3 to 2.1 V/Pt, the oxidation signal is somewhat disturbed, obviously due to oxygen bubbling. This disturbance hinders to expect an accurate calibration of the current peak with the oxide content.

3.2.3. Chronopotentiometry and diffusion coefficient

The diffusion coefficient of the oxide ions in the system LiF-NaF-Li_2O was determined by chronopotentiometry on a gold electrode at 800°C. The chronopotentiogram shown in Figure 4, obtained for an intensity of 25 mA, exhibits a single plateau at about 1.35 V/Pt, which confirms the one-step mechanism previously evidenced by cyclic voltammetry. On Figure 5, the validity of Sand law is verified by plotting the ratio $\frac{I\sqrt{\tau}}{C}$ versus the applied intensity (see equation 1 below), since the ratio is constant for each applied intensity; this result allows concluding that the process is limited by the diffusion of oxide ions into the solution and determining the diffusion coefficient of O^{2-} ions using Sand law:

$$\frac{I\sqrt{\tau}}{C} = 0.5\ n\ F\ S\ \sqrt{\pi D} \qquad (1)$$

where n is the number of exchanged electrons, F the Faraday constant, S the surface area of the electrode, I the applied intensity, τ the transition time, C the active specie content and D the diffusion coefficient.

At 800°C, the diffusion coefficient $D_{O^{2-}}$ was calculated to be (7.90 ± 0.01) 10^{-5} $cm^2\ s^{-1}$.

In the bibliography, K. Grjotheim *et al.* [15] propose the value of 2.0 10^{-5} cm²/s for oxide ions diffusion coefficient in cryolithe melts at 960°C. This value is in the same order of magnitude than the one of the present work; the difference between these values can be explained by the different physicochemical properties of each medium (viscosity, temperature, thermal conductivity).

The calculation of D was repeated at several temperatures. Table 1 reports the obtained values at 750, 800, 840 and 880°C. The evolution of D with temperature obeys the following relationship (Arrenhius' law):

$$D = D° \exp\left(-\frac{E_a}{RT}\right) \qquad (2)$$

where Ea is the activation energy of the diffusion process.

According to Fig. 6, the Eq. (2) can be written as follow:

$$\ln D = 3.6551 - \frac{13968}{T} \qquad (3)$$

where D is in cm²/s, T in K and the activation energy is about 116 kJ/mol.

3.3. Titration of oxide ions using Square Wave Voltammetry

Figure 7 shows a typical square wave voltammogram of the LiF-NaF-Li_2O mixture on a gold electrode, exhibiting a single peak at about 1.4 V/Pt. Notice that its shape is not disturbed by oxygen bubbling which is observed at a more anodic potential, unlike it was

observed on the cyclic voltammogram of Figure 3. Obviously, this peak is associated to the oxidation of oxide ions.

Figure 8 shows that the peak current is linear with the square root of the signal frequency in the 9 – 100 Hz frequency range. This result first confirms the limitation of the electrode process by the diffusion of oxide ions, and then proves that SWV is suitable for a further analysis of the electrochemical system [9;16;17].

This can be verified by measuring the half peak width, $W_{1/2}$, which is correlated to the number of exchanged electrons by the following equation [18;19]:

$$W_{1/2} = 3.52 \frac{RT}{nF} \quad (4)$$

This peak is not exactly symmetric as predicted by several authors such as Osteryoung [20;21]; a similar shape was observed in our previous works in molten fluorides for the reduction of Nd(III) ions to neodymium [22] and in molten chlorides for the reduction of U(III) ions into uranium [23]. In these works, the dissymmetry of the peak was attributed to the nucleation overpotential. Similarly, we assume that the dissymmetry of the peak of Fig. 7 arises most probably of a bubble nucleation effect, the rise of the current being delayed by the overpotential caused by the gaseous phase formation. This explains that the increasing part of the differential current is sharper than the decreasing one. Thus, the disturbance of the signal due to the nucleation effect can be resolved by taking into account only the decreasing part of the peak for the measurement of the half peak width. Accordingly, measuring the half-width of the half peak must be used to calculate n with eq. (4): for three runs, the average value of $W_{1/2}$ is 167 mV; according to Eq. (4), at T = 800 °C, n is found to be 2.10 ± 0.15 as average. The oxidation reaction is then:

$$O^{2-} \rightarrow \frac{1}{2} O_{2\,(g)} + 2\,e^{-} \quad (5)$$

As it is stated that the peak intensity is linear with the electroactive specie content, here the oxide ions, square wave voltammetry is a suitable method for titrating these ions. The linear relationship between the peak current density and the oxide content is evidenced in Figure 9, and the equation of the straight line is:

$$I_p\ (A/cm^2) = 0.353\ [O^{2-}]\ (mol/kg) \qquad (6)$$

This relation allows calculating the free oxide content of a melt by measuring the peak current density obtained by square wave voltammetry at 36 Hz on a gold electrode.

3.4. Residual free oxide ions content determination

This methodology has been applied to estimate the residual free oxide ions content present in fluoride melts at the beginning of the experiment without any thermal pre-treatment during the preparation. Figure 10 shows an example of a square wave voltammogram of a LiF-NaF medium obtained after the fusion without any treatment to remove residual oxide ions at 1100 K with a signal frequency of 36 Hz.

This figure exhibits the oxide ions oxidation peak at 1.4 V/Pt with a current density of $1.1\ 10^{-3}$ $A.cm^{-2}$. Using equation (6), the initial residual oxide ions content of this melt is estimated to be $3.1\ 10^{-3}$ mol/kg.

4. Conclusion

In this work, the electrochemical behaviour of O^{2-} ions was investigated in the LiF/NaF eutectic melt: it was first demonstrated that the oxidation mechanism of O^{2-} ions into oxygen proceeds in a single electrochemical step exchanging 2 electrons and limited by the

diffusion of the specie in the solution. The O^{2-} diffusion coefficient is equal to 7.90 10^{-5} cm^2s^{-1} at 800°C.

Then, the use of square wave voltammetry on a gold electrode for free oxide titration was assessed in the LiF-NaF melt, since a linear relationship between the peak current density and the free oxide content was observed. Consequently, this methodology could be applied either to estimate the purity of a fluoride bath for processes requiring low oxide content (e.g. the electrodeposition of refractory metals), or to monitor the oxide content during electrolyses involving oxide ions as reactant in anodic processes.

References

[1] C. Wagner, *Naturwiss.*, **31** (1943) 265.

[2] J. D. Van Norman and R. A. Osteryoung, *Anal. Chem.*, **32** (1960) 389.

[3] G. Letisse and B. Tremillon, *J. Electroanal. Chem.*, **17** (1968) 387.

[4] B. Tremillon, A. Bermond and R. Molina, *J. Electroanal. Chem.*, **74** (1972) 53.

[5] F. Séon, phD thesis, *University Pierre et Marie Currie*, Paris, France (1981).

[6] B. Lafage and P. Taxil, *J. Electrochem. Soc.* **140(11)** (1993) 3089.

[7] B. Lafage, P. Taxil and T. Tonthat: French patent, Fr 2 700 393, (1993).

[8] P. Chamelot, phD thesis, *University Paul Sabatier*, Toulouse, France (1994).

[9] P. Chamelot, B. Lafage and P. Taxil, *Electrochim. Acta,* **43** (1997) 607.

[10] L. Massot, P. Chamelot, F. Bouyer and P. Taxil, *Electrochim. Acta,* **47** (2002) 1949.

[11] L. Massot, P. Chamelot, F. Bouyer and P. Taxil, *Electrochim. Acta,* **48** (2003) 465.

[12] L. Cassayre, P. Chamelot, L. Aururault, P. Taxil, *J. App. Electrochem.*, **35**(10) (2005) 999.

[13] Y. Berghoute, A. Salmi, F. Lantelme, *J. Electroanal. Chem.* **365** (1994) 171.

[14] Barin, O. Knacke and O. Kubashewski, *Thermochemical properties of inorganic substances*, Springer-Verlag, Berlin (1991).

[15] K. Grjotheim, C. Krohn, M. Malinovsky, K. Matiasovsky and J. Thonstad, *Aluminium Electrolysis, Fundamentals of the Hall-Héroult Process,* 2nd ed., Aluminium-Verlag, Dusseldorf (1982).

[16] P. Chamelot, B. Lafage, P. Taxil, *Electrochim. Acta,* **39** (1994) 2571.

[17] P. Chamelot, P. Palau, L. Massot, A. Savall, P. Taxil, *Electrochim. Acta,* **47** (2002) 3423.

[18] L. E. Ramalay, M. S. Krause, *Anal. Chem.*, **41** (1969) 1362.

[19] L. E. Ramalay, M. S. Krause, *Anal. Chem.*, **41** (1969) 1365.

[20] J. Osteryoung, R. A. Osteryoung, *Anal. Chem*. **57** (1985) 101.

[21] J. Osteryoung, J.J. O'Dea, *J. Electroanal. Chem*., **14** (1986) 209.

[22] C. Hamel, P. Chamelot, P. Taxil, *Electrochim.Acta*, **49** (2004) 4467.

[23] K. Serrano, P. Taxil, *J. Appl. Electrochem*., **29** (1999) 497.

Legends of figures

Fig. 1:

Comparative potential – oxoacidity diagram for oxygen and gold compounds.

Fig. 2:

Typical cyclic voltammogram of the LiF-NaF system at 100mV/s and T = 800°C.

Working El.: Au (S = 0.147 cm²); *Auxiliary El.:* vitreous carbon; *Reference El.:* Pt

Fig. 3:

Evolution of the cyclic voltammograms of the LiF-NaF-Li_2O system at 100mV/s and T = 800°C for various oxide ions contents.

Working El.: Au (S = 0.147 cm²); *Auxiliary El.:* vitreous carbon; *Reference El.:* Pt

Fig. 4:

Typical chronopotentiogram of the LiF-NaF-Li_2O ($9.41\ 10^{-5}$ mol/ml) system at T = 800°C. Applied intensity 25 mA.

Working El.: Au (S = 0.16 cm²); *Auxiliary El.:* vitreous carbon; *Reference El.:* Pt

Fig. 5:

Evolution of $I\tau^{1/2}$ /C vs. the intensity at 800°C.

Working El.: Au (S = 0.16 cm²); *Auxiliary El.:* vitreous carbon; *Reference El.:* Pt

Fig. 6:

Linear relationship of the logarithm of O^{2-} diffusion coefficient vs. the reciprocal of the absolute temperature.

Working El.: Au (S = 0.16 cm²); *Auxiliary El.:* vitreous carbon; *Reference El.:* Pt

Fig. 7:

Square wave voltammogram of the LiF-NaF-Li_2O (9.41 10^{-5} mol/ml) system at 36 Hz and T = 800°C.

Working El.: Au (S = 0.147 cm²); *Auxiliary El.:* vitreous carbon; *Reference El.:* Pt

Fig. 8:

Linear relationship of the peak current density versus the square root of the frequency of the LiF-NaF-Li_2O (9.41 10^{-5} mol/ml) system at 100mV/s and T = 800°C.

Working El.: Au (S = 0.147 cm²); *Auxiliary El.:* vitreous carbon; *Reference El.:* Pt

Fig. 9:

Linear relationship of the peak current density versus oxide ion content, obtained by square wave voltammetry, of the LiF-NaF-Li_2O system at T = 800°C for various oxide ion additions.

Working El.: Au (S = 0.147 cm²); *Auxiliary El.:* vitreous carbon; *Reference El.:* Pt

Fig. 10:

Square wave voltammogram of a LiF-NaF medium without any oxide addition and treatment at 36 Hz and T = 800°C.

Working El.: Au (S = 0.147 cm²); *Auxiliary El.:* vitreous carbon; *Reference El.:* Pt

Table 1:

Evolution of the O^{2-} diffusion coefficient with the temperature.

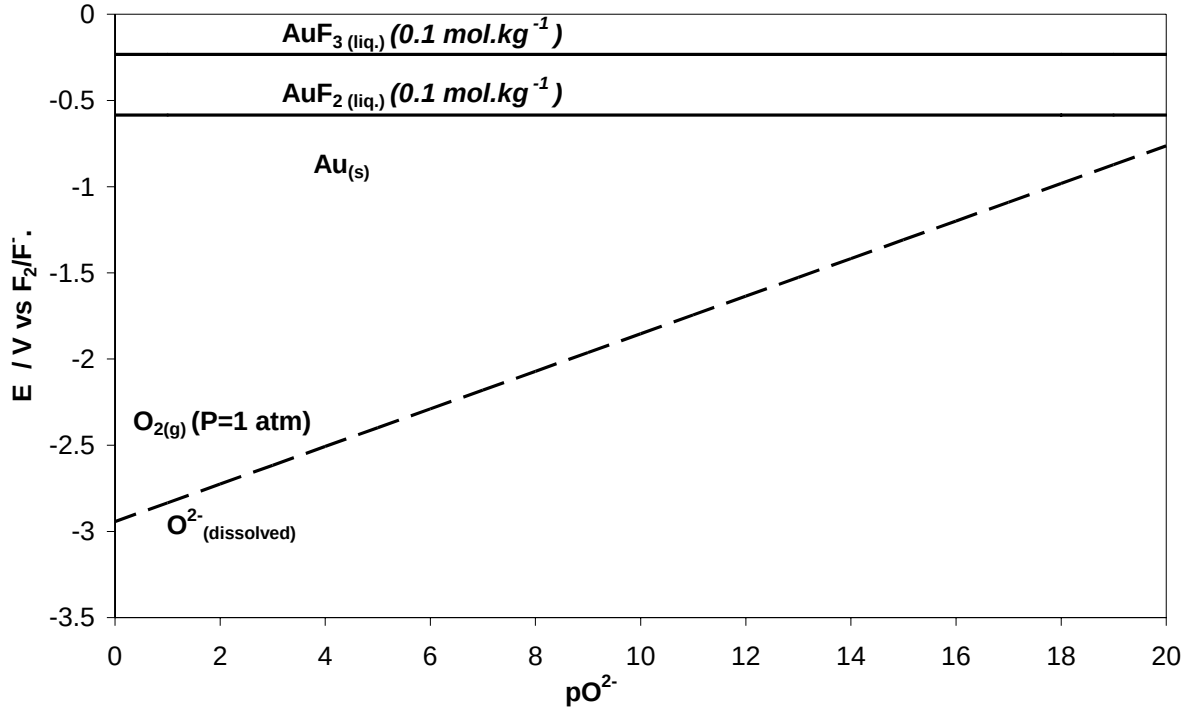
AuF3 (liq.) (0.1 mol.kg-1)
AuF2 (liq.) (0.1 mol.kg-1)
Au(s)
O2(g) (P=1 atm)
O2- (dissolved)
E / V vs F2/F-.
pO2-
0
-0.5
-1
-1.5
-2
-2.5
-3
-3.5
0
2
4
6
8
10
12
14
16
18
20

Figure 1

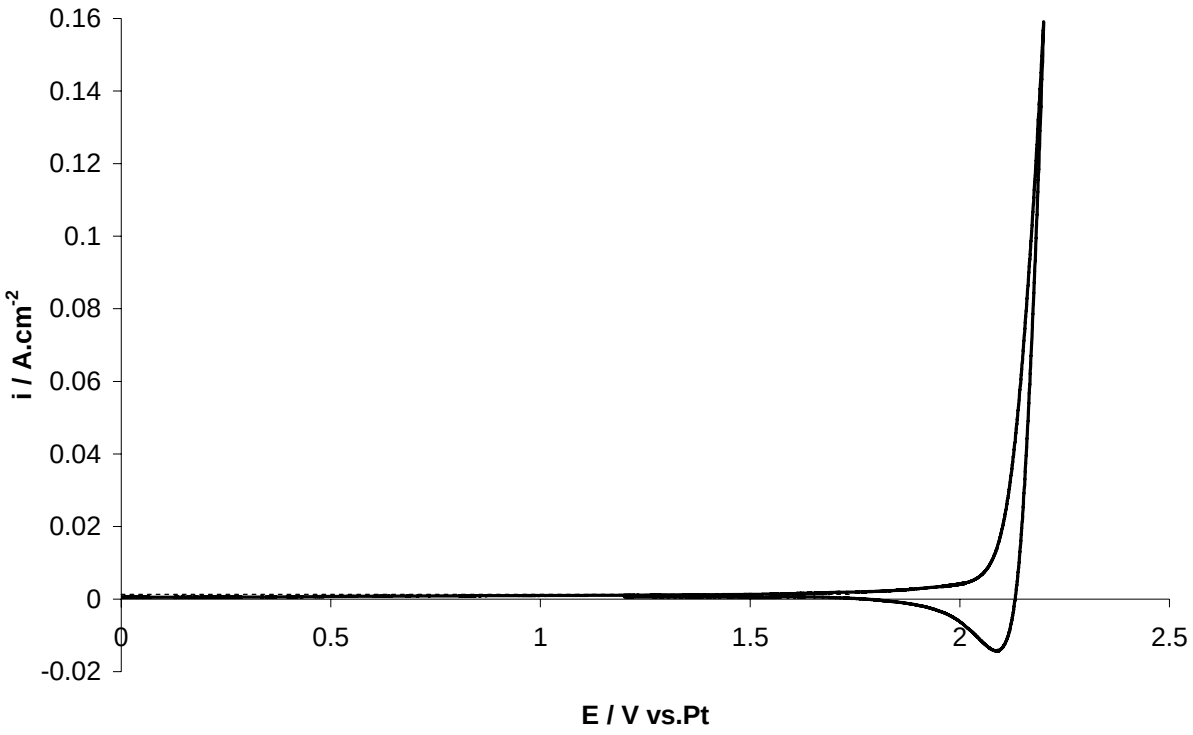

Figure 2

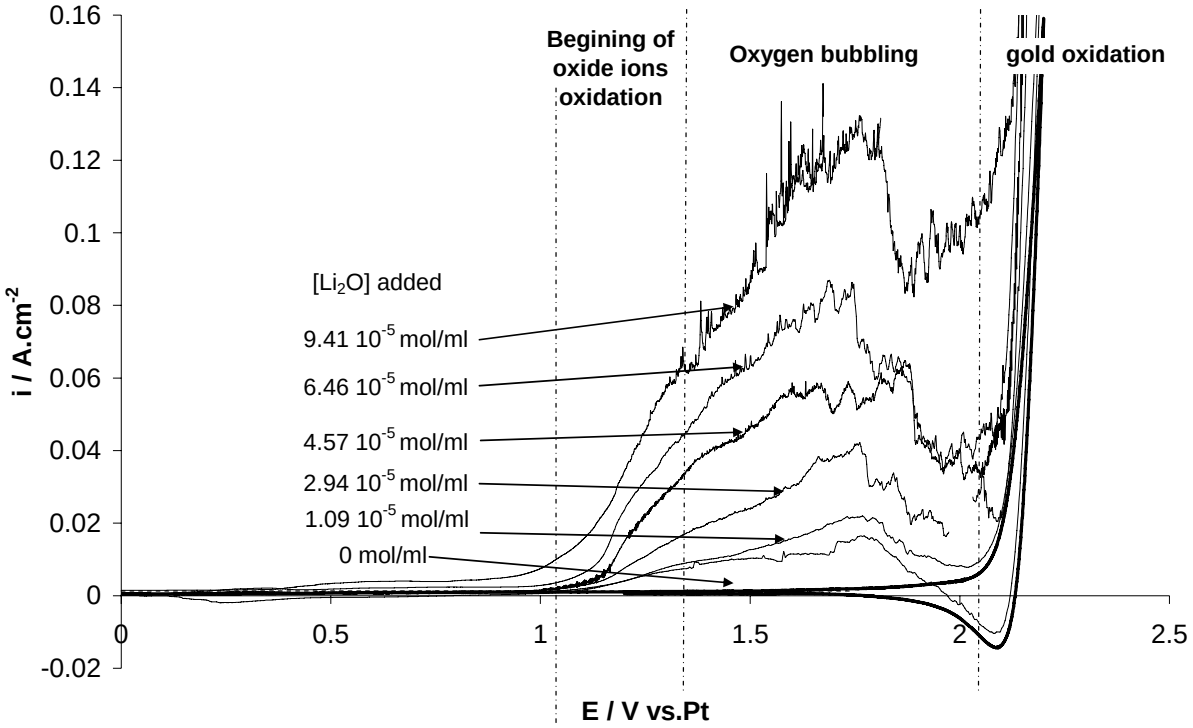
Begining of oxide ions oxidation
Oxygen bubbling
gold oxidation
[Li2O] added
9.41 10-5 mol/ml
6.46 10-5 mol/ml
4.57 10-5 mol/ml
2.94 10-5 mol/ml
1.09 10-5 mol/ml
0 mol/ml
i / A.cm-2
E / V vs.Pt
0.16
0.14
0.12
0.1
0.08
0.06
0.04
0.02
0
-0.02
0
0.5
1
1.5
2
2.5

Figure 3

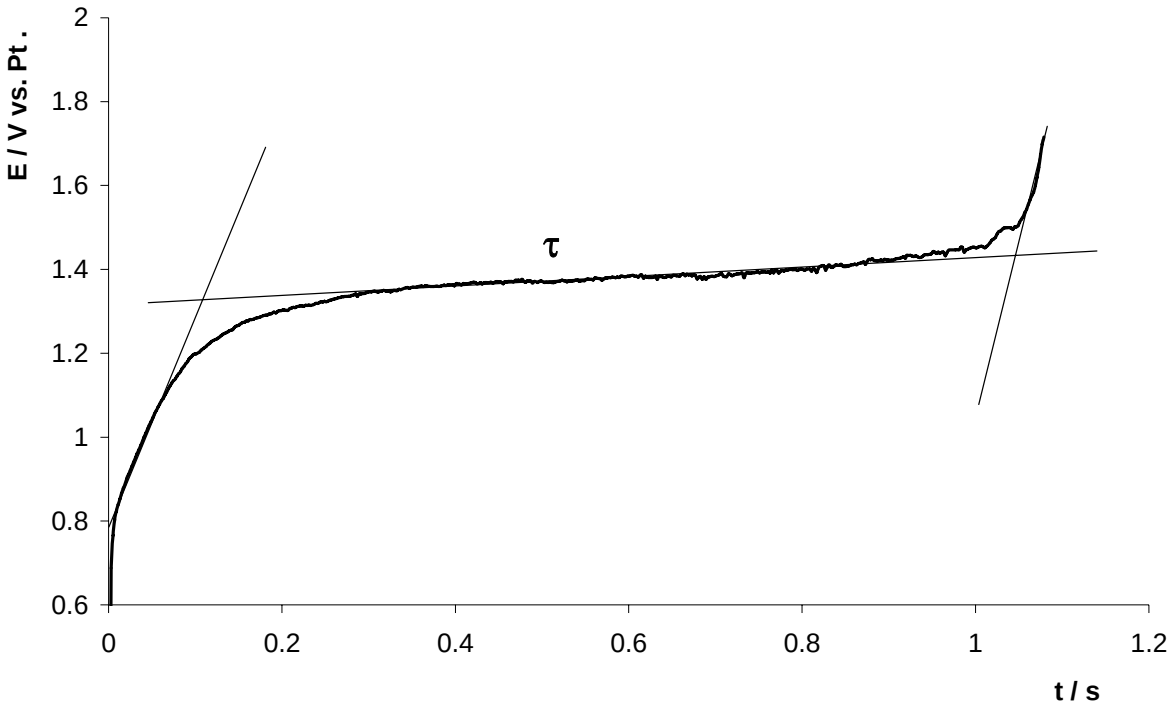

Figure 4

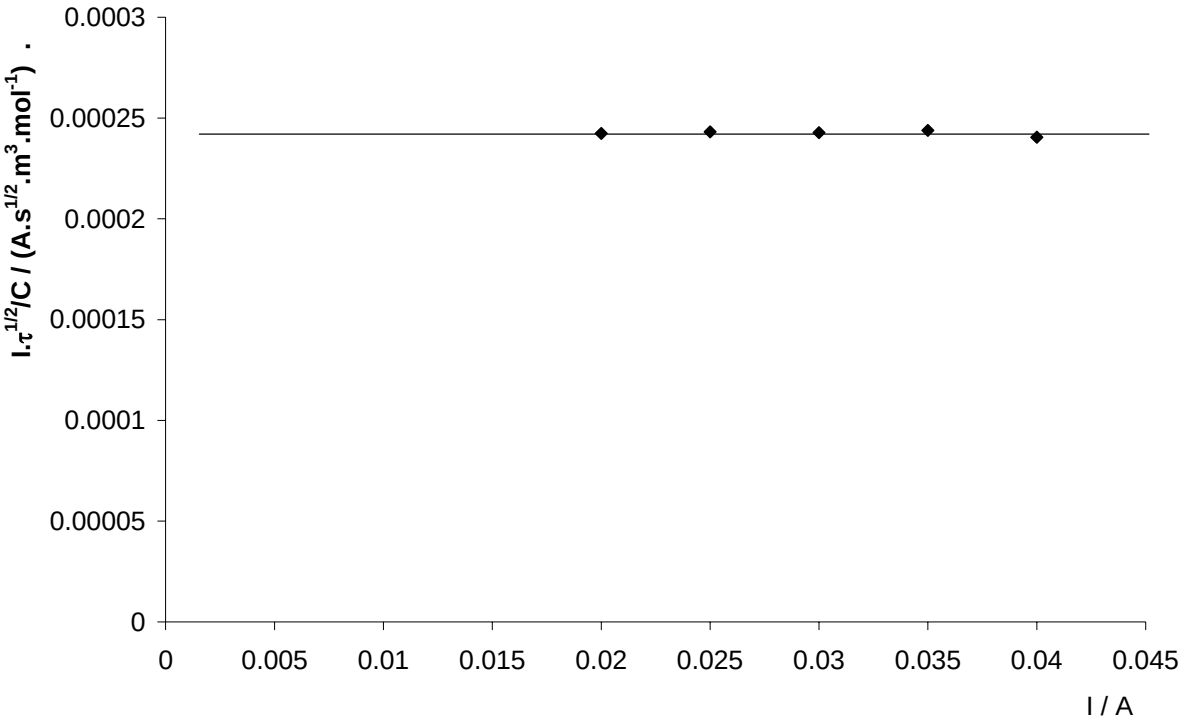
0.0003
0.00025
0.0002
0.00015
0.0001
0.00005
0
0
0.005
0.01
0.015
0.02
0.025
0.03
0.035
0.04
0.045
I / A
I.τ^1/2/C / (A.s^1/2.m^3.mol^-1) .

Figure 5

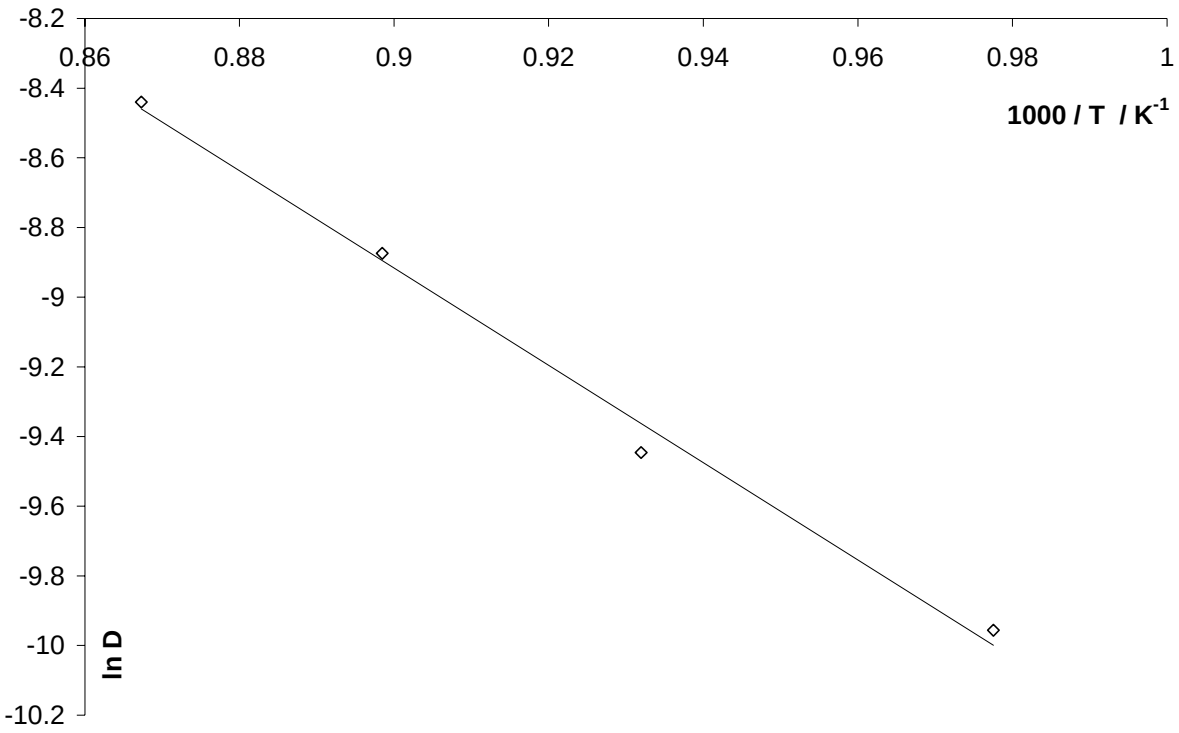
-8.2
0.86
0.88
0.9
0.92
0.94
0.96
0.98
1
-8.4
-8.6
-8.8
-9
-9.2
-9.4
-9.6
-9.8
-10
-10.2
1000 / T / K-1
ln D

Figure 6

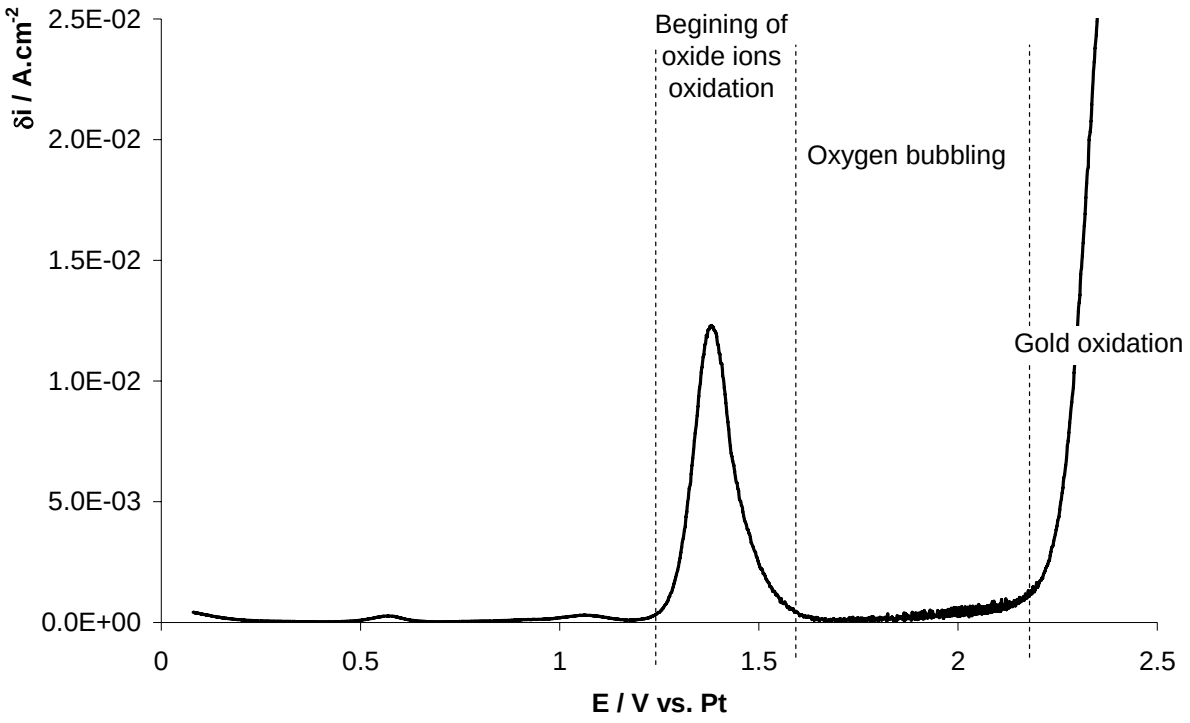
δi / A.cm-2
2.5E-02
2.0E-02
1.5E-02
1.0E-02
5.0E-03
0.0E+00
0
0.5
1
1.5
2
2.5
E / V vs. Pt
Begining of oxide ions oxidation
Oxygen bubbling
Gold oxidation

Figure 7

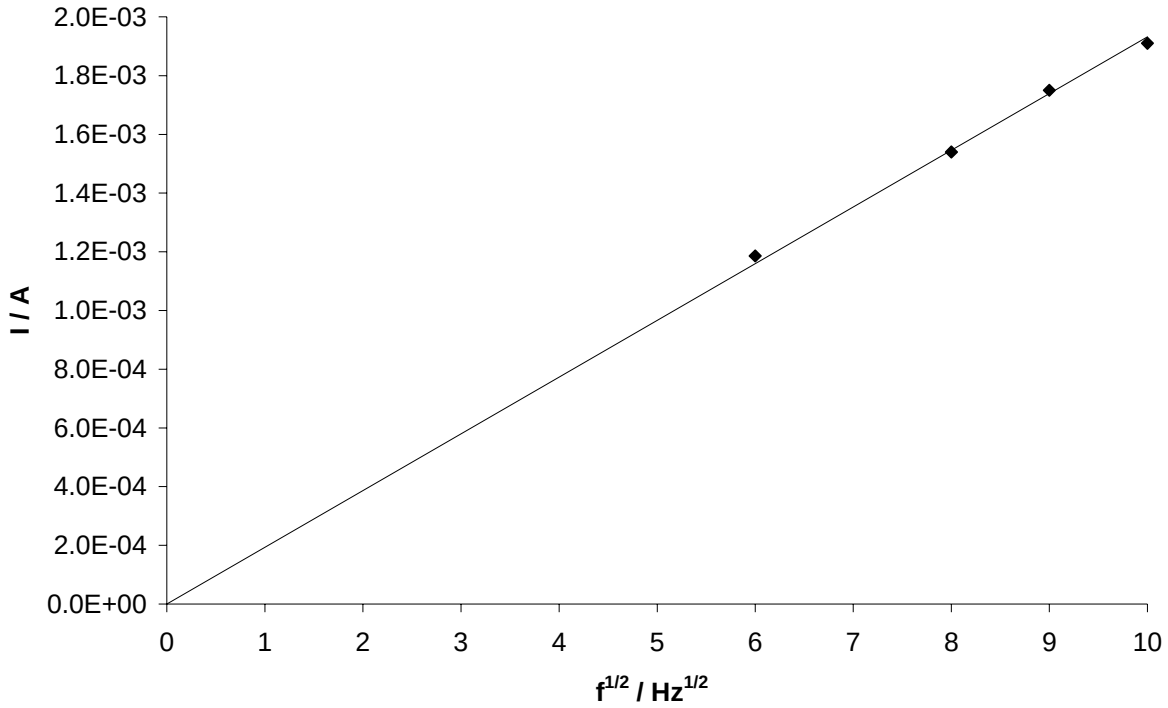
2.0E-03
1.8E-03
1.6E-03
1.4E-03
1.2E-03
1.0E-03
8.0E-04
6.0E-04
4.0E-04
2.0E-04
0.0E+00
I / A
0
1
2
3
4
5
6
7
8
9
10
f1/2 / Hz1/2

Figure 8

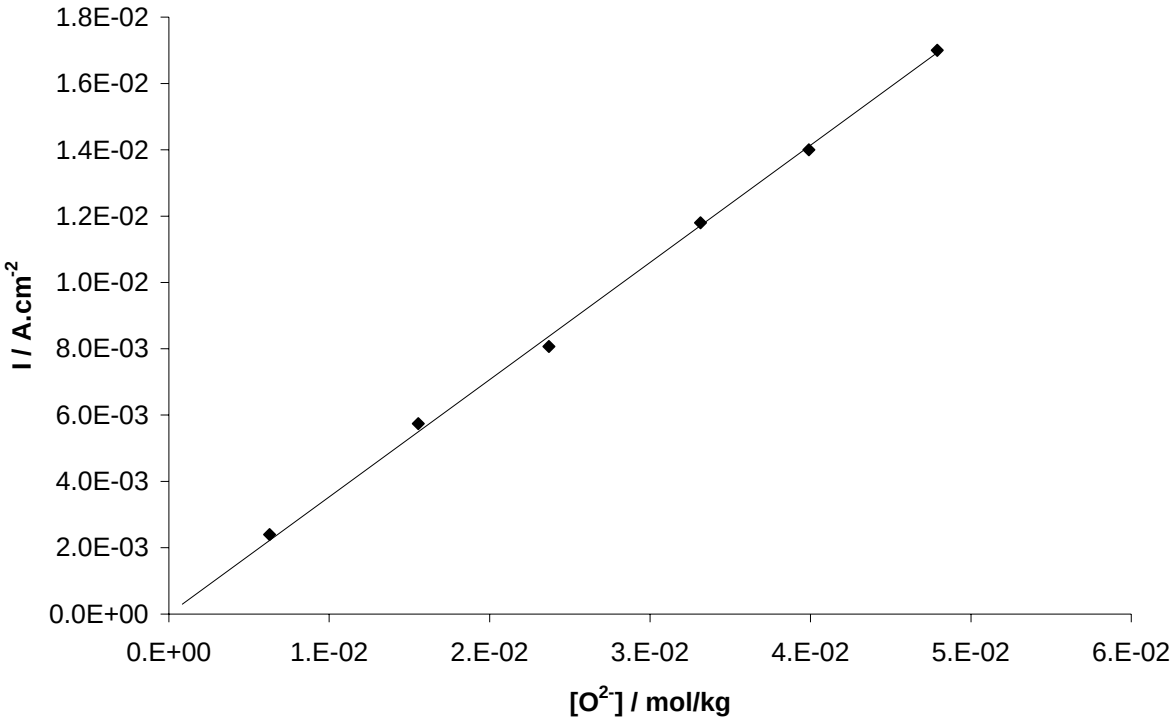
1.8E-02
1.6E-02
1.4E-02
1.2E-02
1.0E-02
8.0E-03
6.0E-03
4.0E-03
2.0E-03
0.0E+00
I / A.cm-2
0.E+00
1.E-02
2.E-02
3.E-02
4.E-02
5.E-02
6.E-02
[O2-] / mol/kg

Figure 9

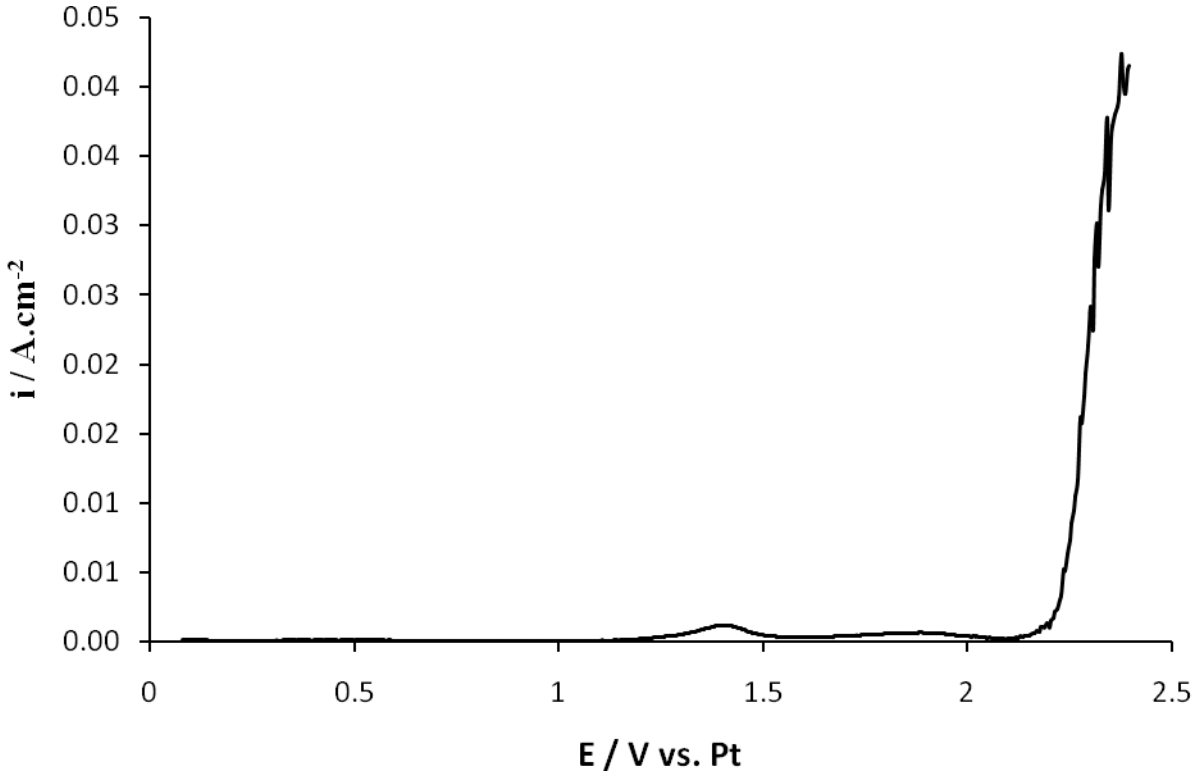
0.05
0.04
0.04
0.03
0.03
0.02
0.02
0.01
0.01
0.00
i / A.cm-2
0
0.5
1
1.5
2
2.5
E / V vs. Pt

Figure 10

Temperature (°C)	D * 10^5 (cm²/s)
750	4.74
800	7.90
840	14.0
880	21.6

Table 1